ACKNOWLEDGMENT

Support of the simulation tools from the National Center for High Performance Computing, Hsinchu, Taiwan is acknowledged.

REFERENCES

[1] C. Y. Huang and K. L. Wong, "Stripline-fed printed square spiral slot antenna for circular polarisation," *Electron. Lett.*, vol. 34, no. 24, pp. 2290–2292, Nov. 1998.

[2] S. Shi, K. Hirasawa, and Z. N. Chen, "Circularly polarized rectangularly bent slot antennas backed by a rectangular cavity," *IEEE Trans. Antennas Propag.*, vol. 49, no. 11, pp. 1517–1524, Nov. 2001.

[3] K. L. Wong, C. C. Huang, and W. S. Chen, "Printed ring slot antenna for circular polarization," *IEEE Trans. Antennas Propag.*, vol. 50, no. 1, pp. 75–77, Jan. 2002.

[4] K. M. Chang, R. J. Lin, I. C. Deng, J. B. Chen, K. Q. Xiang, and C. J. Rong, "A novel design of a CPW-fed square slot antenna with broadband circular polarization," *Microw. Opt. Technol. Lett.*, vol. 48, no. 12, pp. 2456–2459, Dec. 2006.

[5] I. C. Deng, J. B. Chen, Q. X. Ke, C. J. Rong, W. F. Chang, and Y. T. King, "A circular CPW-fed slot antenna for broadband circularly polarized radiation," *Microw. Opt. Technol. Lett.*, vol. 49, no. 11, pp. 2728–2733, Nov. 2007.

[6] I. C. Deng, K. Q. X. Ke, R. J. Lin, and Y. T. King, "A circular CPW-fed slot antenna resonated by the circular loop for broadband circularly polarized radiation," *Microw. Opt. Technol. Lett.*, vol. 50, no. 5, pp. 1423–1426, May 2008.

[7] S. L. S. Yang, A. A. Kishk, and K. F. Lee, "Wideband circularly polarized antenna with L-shaped slot," *IEEE Trans. Antennas Propag.*, vol. 56, no. 6, pp. 1780–1783, Jun. 2008.

[8] C. J. Wang and W. T. Tsai, "A stair-shaped slot antenna for the triple-band WLAN applications," *Microw. Opt. Technol. Lett.*, vol. 39, no. 5, pp. 370–372, Dec. 2003.

Interleaved Array Antennas for FMCW Radar Applications

Ioan E. Lager, Christian Trampuz, Massimiliano Simeoni, and Leonardus P. Ligthart

***Abstract*—An effective and robust strategy for concurrently designing the transmit and receive antennas of a frequency-modulated, continuos-wave radar is discussed. The aperture architecture is based on the use of non-periodic, interleaved sub-arrays. Deterministic element placement is employed for ensuring design efficiency. The procedure yields controllable sub-array radiation patterns and two-way side-lobe levels below −30 dB, that are also stable over a wide frequency range.**

***Index Terms*—Antenna arrays, array interleaving, frequency-modulated, continuos-wave (FMCW) radar.**

I. INTRODUCTION

Interleaving non-periodic sub-arrays provides a powerful and versatile tool to implement multifunctionality in antenna systems [1]–[3]. One of the yet unexplored potentialities of this architecture is its intrinsic capability to attenuate the system phase noise in frequency-modulated, continuos-wave (FMCW) radars, a feature that is determinant for ensuring the system's ability to identify targets [4]. By virtually collocating the transmit (T) and receive (R) antennas, interleaving yields a substantial reduction of the signal leakage paths and, thus, phase noise suppression.[1] At the same time, as in any radar application, the FMCW front-end needs ensuring low side-lobe levels (SLL) and, frequently, narrow beamwidths. Addressing simultaneously these complex, highly demanding desiderata requires elaborate and often time-consuming design strategies.

One of the favored options for resolving the interleaving of sub-arrays is by invoking stochastic optimization techniques, [1] providing an example of using the genetic algorithm to this end. While allowing for more flexibility in defining cost functions and creating conditions for determining global optima, the statistical optimization carries very large or even impractical computational costs, as indicated in the conclusions of [1]. A viable alternative for greatly increasing the design process efficiency is offered by the deterministic placement strategies, a particularly expedient physical implementation of the concept being the one demonstrated in [2]. In it, an initial uniform two-dimensional array with constant half-wavelength spacing is thinned by means of the strategy described in [6], a method that exploits the convenient properties of the cyclic difference sets (CDS) [7, Ch. 7]. Note that, unlike other thinning techniques, the one advocated in [6] guarantees the grating-lobes-free operation and the average SLL for both the sub-array consisting of the retained elements and for its complement, consisting of the eliminated ones. Since the method yields, in fact, two independently usable, fully disjoint sub-arrays, it actually performs a *complementary division* of the initial fully populated aperture. This feature was used in [2] for designing a multifrequency array antenna.

The present contribution discusses the design of a shared aperture consisting of two interleaved sub-arrays that are taken to represent the T and R antennas of an FMCW radar system. After complementarily dividing a fully populated array antenna into two well-balanced sub-arrays, an effective artifice is employed for reducing the peak SLL by 6 dB. The favorable radiation properties of the system are demonstrated to be stable over a wide frequency range.

II. PREREQUISITES

The examined configurations are considered with respect to a Cartesian frame $Oxyz$. The shared aperture is located in the xOy plane and radiates into the half-space $\{z > 0\}$ where the medium is taken to be vacuum. The far-field quantities are expressed with respect to a polar reference frame $Or\vartheta\varphi$, with $\vartheta(0 \leqslant \vartheta \leqslant \pi)$ measuring the tilting with respect to Oz, and $\varphi(0 \leqslant \varphi < 2\pi)$ measuring the rotation from Ox in xOy. The planes $\{\varphi = 0 \cup \varphi = \pi\}$ and $\{\varphi = \pi/2 \cup \varphi = 3\pi/2\}$ will be referred to as the H- and E-planes, respectively.[2]

Since the present work focuses on an FMCW radar application, *two-way* front-end parameters, defined with respect to the product T-R radiation patterns, are applicable. The required two-way, half-power beamwidths are $\vartheta^{\mathrm{H}}_{\rightleftarrows,1/2} \leqslant 0.9^\circ$ in the H-plane and $6.5^\circ \leqslant \vartheta^{\mathrm{E}}_{\rightleftarrows,1/2} \leqslant 10^\circ$ in the E-plane. Assuming that the antenna is mechanically rotated, no electronic beam steering is required and the sub-arrays are designed for broadside radiation. The center operating

Manuscript received April 22, 2008; revised August 27, 2008. First published June 05, 2009; current version published August 05, 2009.

The authors are with the International Research Centre for Telecommunications and Radar (IRCTR), Delft University of Technology, 2628 CD Delft, the Netherlands (e-mail: i.e.lager@tudelft.nl; c.trampuz@tudelft.nl; m.simeoni@tudelft.nl; l.p.ligthart@tudelft.nl).

Color versions of one or more of the figures in this paper are available online at http://ieeexplore.ieee.org.

Digital Object Identifier 10.1109/TAP.2009.2024573

[1] With reference to [5, pp. 14.5–14.6], shortening the relevant path by a factor of 10 yields a 20 dB reduction in the system phase noise level.

[2] For simplifying the notation in the plots depicting ϑ dependencies in the H- and E-planes, the ϑ coordinate will be conventionally taken to assume negative values in the half-planes where $\varphi \geqslant \pi$.

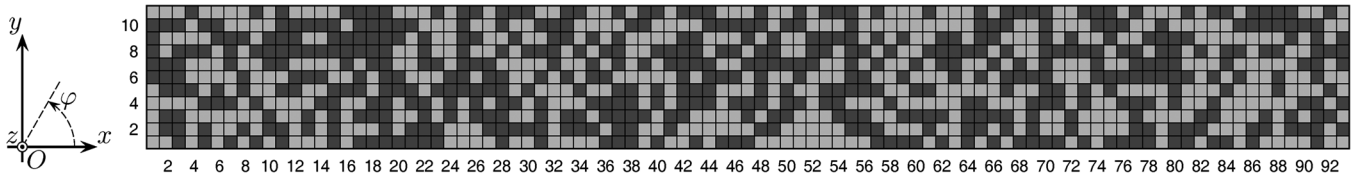

Fig. 1. The radiating aperture's architecture. The dark squares correspond to the T sub-array and the light ones to the R sub-array.

frequency is taken to be $f_c = 9.4$ GHz, the full chirp amounting to 50 MHz.

III. Complete, Interleaved Sub-Arrays

As a first step, a pair of interleaved sub-arrays is designed such that to ensure the following characteristics: the required beamwidths, similar overall radiation patterns, a grating-lobes-free operation and a (reasonably) low SLL. It is also desirable to utilize completely the available real estate and to maintain the balance between the number of elements in the sub-arrays.

These concurrent objectives are effectively attained by assigning the elements in an initial uniform, fully populated array according to the thinning strategy described in [6]. In that work it was demonstrated that: (i) the two-valued autocorrelation property of the CDS yields a predictable *average* SLL for the thinned array; (ii) the grating-lobes-free operation of the initial array is preserved for the thinned one; (iii) the properties that hold for the array consisting of the retained elements are also valid for that consisting of the removed ones. The placement method then allows performing a *complementary division* of the initial array into two sub-arrays with similar and predictable properties. The only ingredient still needed is identifying a CDS that partitions the elements in a balanced manner. It is stressed that other placement techniques that yield interleaved arrays complying with the requirements in the first paragraph of this section are also eligible for designing the shared aperture. Nevertheless, the predictability and computational efficiency of the CDS based strategy provide strong arguments for making it the method of choice in this work.

The initial array is cast on an orthogonal, uniform, $\lambda_c/2$-spaced lattice, with λ_c denoting the free space wavelength at f_c. The elementary radiators are taken to be dielectrically filled, flanged, rectangular waveguide-ends of dimensions 10.9 mm × 4.8 mm, the relative permittivity of the dielectric amounting to 3.38. The assessment of the sub-array performance is based on the corresponding radiation patterns that are calculated by means of pattern multiplication [8, Chapter 6]. For stressing the intrinsic features of the hereby proposed design strategy, the effect of the mutual coupling is deliberately not accounted for in the present study.

The lattice dimensions are chosen as 11 × 93 that, by invoking the arguments in [8, pp. 260–261], are deemed to ensure the required half-power beamwidths while, at the same time, allow using the {1023,511,255} CDS [9], [10] as a blueprint. The effect on the shared aperture radiation properties of using as placement template any of the 10 available variants of that CDS, each of which in conjunction with all possible cyclic shifts, was examined. The numerical experiments evidenced some variations in the side-lobe distribution but in regions where the SLL was however very low. No significant influence on the half-power beamwidths and on the peak SLL was observed. For being able to assess the improvement achieved by applying the technique that will be described in Section IV, the results of the numerical experiments concerning the cyclically shifted by 18, [0,1,2,4,7,8,9,...] variant of the {1023,511,255} CDS [10] are hereafter catalogued.

The completely assembled shared aperture antenna is depicted in Fig. 1. The initial array is divided into a T sub-array containing 511 of the total 1023 elements (49.95%) and an R sub-array containing the remaining 512 ones (50.05%). Note that these ratios, deriving from the intrinsic properties of the employed CDS, are the same for any of the existing 10 variants and for any cyclic shift.

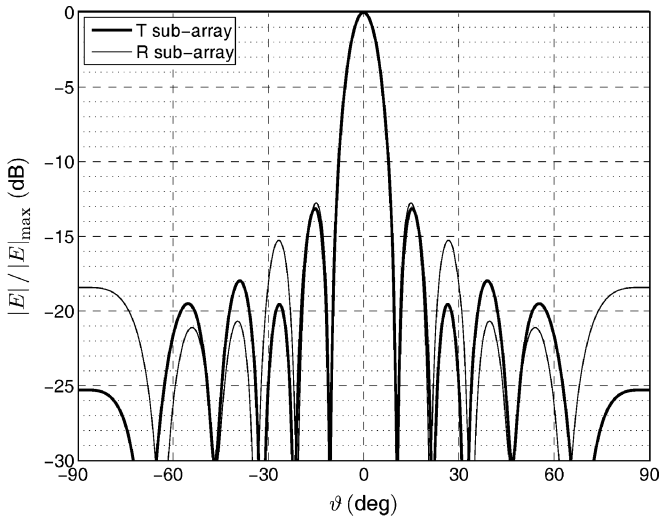

Fig. 2. The normalized sub-array patterns in the E-plane.

The corresponding sub-array radiation patterns in the E- and H-planes are presented in Figs. 2 and 3, respectively, with $\boldsymbol{E}$ being representative for the electric field strength radiated by either the T sub-array ($\boldsymbol{E}^{\mathrm{T}}$) or the R sub-array ($\boldsymbol{E}^{\mathrm{R}}$). From these figures it is clear that the CDS based placement strategy yields sub-arrays with remarkably similar patterns.

Recall now that the front-end specifications were given in Section II for the complete T-R system. In order to obtain the two-way performance, the computed sub-array radiation patterns are multiplied, the result of this operation being displayed in Figs. 4 and 5 for the E- and H-planes, respectively, with $P = |\boldsymbol{E}^{\mathrm{T}}||\boldsymbol{E}^{\mathrm{R}}|$. From these plots, it can be derived that the corresponding two-way half-power beamwidths amount to $\vartheta^{\mathrm{E}}_{\rightleftarrows,1/2} = 6.67^\circ$ and $\vartheta^{\mathrm{H}}_{\rightleftarrows,1/2} = 0.78^\circ$, values that comply with the imposed specifications.

A key figure of merit in radar applications is the two-way SLL, hereafter referred to as $\mathrm{SLL}_{\rightleftarrows}$. Its peak value (denoted as $\mathrm{pSLL}_{\rightleftarrows}$) corresponds to the "M" markers in Figs. 4 and 5, reaching $\mathrm{pSLL}^{\mathrm{E}}_{\rightleftarrows} = -25.92$ dB and $\mathrm{pSLL}^{\mathrm{H}}_{\rightleftarrows} = -26.57$ dB in the E- and H-planes, respectively. The observed levels are rather modest for the application at hand and solutions for reducing them must be called upon. It is noted that these levels represent, roughly, twice the peak SLL obtained when using uniform, linear arrays [8, p. 261], namely $2 \times (-13.26)$ dB. Furthermore, and not surprisingly, both top values correspond to the first side-lobes, that would also be the case with uniform, linear arrays. This observation will be conducive for devising a strategy to significantly reduce the $\mathrm{pSLL}_{\rightleftarrows}$.

IV. Trimmed, Interleaved Sub-Arrays

In view of reducing the $\mathrm{pSLL}_{\rightleftarrows}$, it is firstly noted that the sub-array radiation patterns have very similar main beams and overall side-lobe

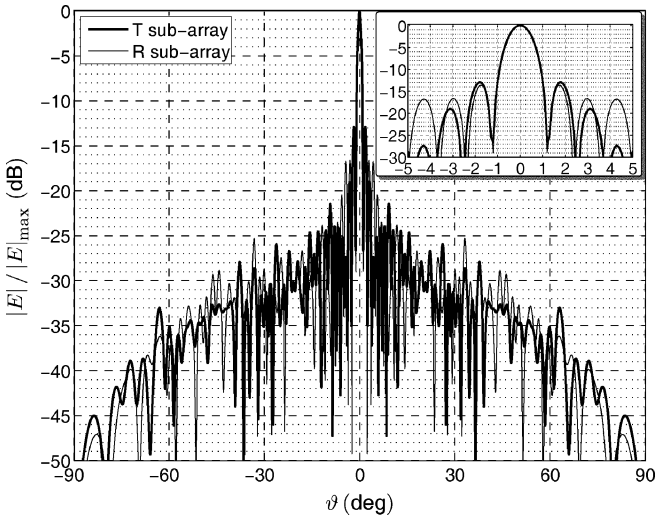

Fig. 3. The normalized sub-array patterns in the H-plane. The inset depicts a zoom-in on the main beam.

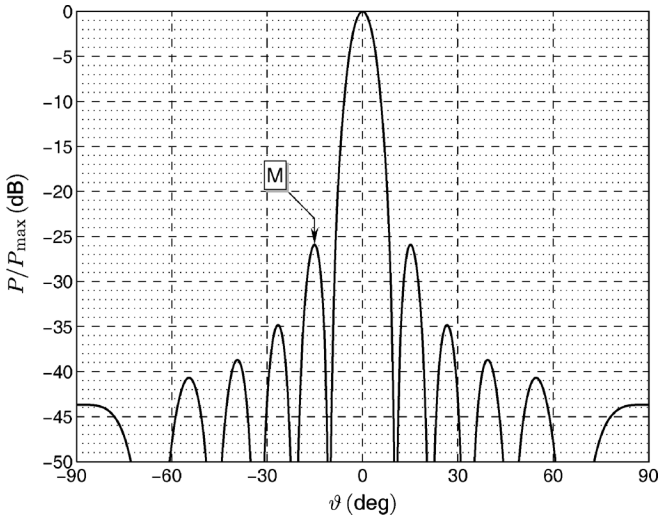

Fig. 4. The normalized, two-way pattern in the E-plane.

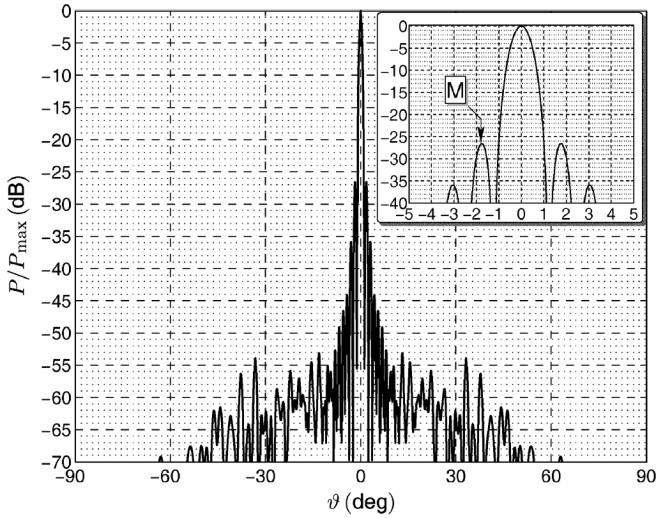

Fig. 5. The normalized, two-way pattern in the H-plane. The inset depicts a zoom-in on the main beam.

distribution. Obviously, these beneficial features of the T and R front-ends should be preserved. Secondly, as stated in the concluding part of Section III, the performance of the two sub-arrays resembles in the vicinity of the main beam that of uniform, linear arrays.

With these observations in mind, consider now the case of the array factor characterizing a uniform, $\lambda/2$-spaced, broadside, linear array. The angles $\vartheta_{\mathrm{pSLL}}$ at which the $\mathrm{pSLL}_{\rightleftarrows}$ occurs have the values [8, p. 261]

$$\vartheta_{\mathrm{pSLL}} = \pm \arcsin\left(\frac{3}{N}\right) \tag{1}$$

where N denotes the number of elements in the linear array. Note that N can be assimilated, in the case of the examined interleaved sub-arrays, to the *number of columns* for the array factor in the H-plane and to the *number of rows* for the array factor in the E-plane. Furthermore, the array factor nulls occur at the angles [8, p. 260]

$$\vartheta_i = \pm \arcsin\left(\frac{2i}{N}\right), \quad \text{for } i = 1, \ldots, N-1. \tag{2}$$

By corroborating (1) and (2) with $i = 1,2$, it can be inferred that the first side-lobes will, by and large, overlap as long as N is the same in the two sub-arrays, yielding the already evidenced $\mathrm{pSLL}_{\rightleftarrows}$ of approximately $2 \times (-13.26)$ dB.

It then follows that shifting the first side-lobes in *one* of the sub-arrays seems the only feasible option for modifying the $\mathrm{pSLL}_{\rightleftarrows}$. This shifting can be easily obtained by changing the number of columns or rows, as applicable. It must be stressed that a change of the relevant N will automatically yield a modification of the half-power beamwidth corresponding to that sub-array (see [8, pp. 260–261]).

A number of choices is needed at this point. The CDS placement strategy offered the starting point for meeting the beamwidth specifications and guaranteed the grating-lobes-free operation, and reusing its results is highly desirable. Then, since deterministic placement outside the 11×93 lattice, where no CDS template is available, is not possible, it follows that the relevant N can only be reduced. This reduction can be achieved by eliminating a number of columns or rows at the edges of *one* of the previously generated sub-arrays. It is reasonable to require the two sub-arrays to be modified in a balanced manner and, thus, rows will be removed from one sub-array, yielding a shift of side-lobes in the E-plane, and columns from the other one, yielding a shift in the H-plane. Furthermore, the trimming should be preferably effectuated in a symmetric manner. To conclude with, in order to preclude an unacceptable beamwidth enlargement, the trimming must be limited. Note that an extension of the initial (untrimmed) shared aperture is not possible, the {1023,511,255} CDS being the largest available CDS [10].

These principles are employed for adjusting the fully populated, shared aperture assembled in Section III. Here, a choice is made for columns to be removed from the R sub-array and rows from the T one. Nevertheless, alternatives are possible, the particular selection of the sub-array(s) to be trimmed being dictated by the specificity of the supported application. For the present choice, the large number of columns of the complete aperture allows for a facile symmetric column trimming, while small asymmetries in the row trimming are tolerated due to the reduced initial number of rows.

Preliminary experiments have shown that the effect of the column trimming becomes significant when 2×10 columns are removed, it peaks, and then starts to diminish for 2×14, rendering a further reduction impractical. Consequently, 10 and 14 are adopted as limits of

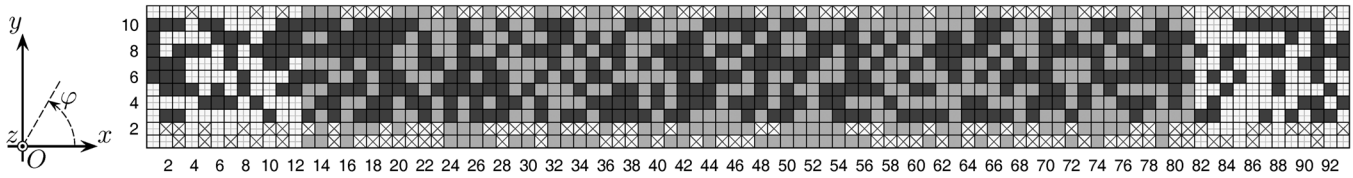

Fig. 6. The radiating aperture's architecture after trimming. The dark squares correspond to the T sub-array and the light ones to the R sub-array. The crosses indicate the switched off elements in the T sub-array and the pluses the switched off elements in the R one.

the examined domain in the optimization procedure to follow. A similar reasoning yields 2 and 4 as the feasible limits for the row trimming. The next step consists of identifying the suitable combination of CDS variant, cyclic shift and column/row trimming that yields the best $\mathrm{pSLL}_{\rightleftarrows}$. A grid search over the 10 available {1023,511,255} CDS variants [10], 1022 possible shifts and the previously indicated [10,14] columns $\times$ [2,4] rows trimming domain is carried out to this end. Note that the Matlab code carrying out the full scan over all CDS variants and shifts for each of the 15 column/row combinations is executed on a 2.39 GHz personal computer in 2 minutes and 20 seconds. For each such scan, the combinations providing the best 10 $\mathrm{pSLL}_{\rightleftarrows}$ in the H-plane are retained, their complete radiation patterns being then inspected visually.

Eventually, the case when 2×12 columns and 3 rows are removed from the initial array that is generated by using the [0,1,2,4,7,8,9,...] variant of the {1023,511,255} CDS, with a cyclic shift by 18, is selected as the optimal solution. The resulting shared aperture architecture is depicted in Fig. 6. When compared with the full aperture, a number of 135 elements are removed from the original 511 in the T sub-array, and 145 from the original 512 in the R sub-array. The additional thinning amounts to 26.42% and 28.32%, respectively. Note that the trimming is carried out in a reasonably balanced manner, as stated in one of the previously enunciated principles. It needs being stressed that the trimming obviously results in a gain reduction. This effect can be compensated in the case of the application at hand by adjusting the parameters of the employed T-R modules.

The radiation patterns of the trimmed sub-arrays are presented in Figs. 7 and 8 for the E- and H-planes, respectively. Note that, although removing elements should, in principle, affect the two-valued autocorrelation properties of the resulting array, no adverse effects are visible in the radiation patterns. The two-way radiation patterns are shown in Figs. 9 and 10. The two-way, half-power beamwidths amount to $\vartheta^{\mathrm{E}}_{\rightleftarrows,1/2} = 7.57^\circ$ and $\vartheta^{\mathrm{H}}_{\rightleftarrows,1/2} = 0.9^\circ$, still complying with the specifications. As for the $\mathrm{pSLL}_{\rightleftarrows}$, the relevant values are $\mathrm{pSLL}^{\mathrm{E}}_{\rightleftarrows} = -29.86$ dB and $\mathrm{pSLL}^{\mathrm{H}}_{\rightleftarrows} = -32.75$ dB, reductions by about 4 dB and 6.2 dB with respect to the levels found for the complete array being recorded, respectively. The suitability of the obtained two-way performance is further proven by studying the $P/P_{\max}$ ratio over all $\{\vartheta, \varphi\}$ directions (see Fig. 11). In view of this quantity being below -40 dB for $\vartheta \geqslant 30^\circ$, that region is clipped out for enhanced plot readability. From Fig. 11 it is clear that, despite the highly irregular element placement, with inter-element spacing significantly exceeding $\lambda_c/2$, no high side-lobes appear in directions that were not accounted for in the optimization procedure, the $\mathrm{pSLL}_{\rightleftarrows}$ occurring in the E-plane. These results demonstrate the effectiveness of the proposed design strategy for reducing the $\mathrm{pSLL}_{\rightleftarrows}$ characteristic of the FMCW radar system.

Finally, the variation of the beamwidth and of the $\mathrm{pSLL}_{\rightleftarrows}$ over the frequency range 9 GHz,...,10 GHz (widely enclosing the envisaged full chirp of 50 MHz) is studied. The former parameter is, practically, constant in both the E- and the H-planes, complying, thus, with the specifications stated in Section II. Upon turning to the $\mathrm{pSLL}_{\rightleftarrows}$, the variation of its normalized value is presented in Fig. 12, in which ϑ_M is the angle corresponding to the "M" markers in Figs. 9 and 10. $\mathrm{pSLL}_{\rightleftarrows}$

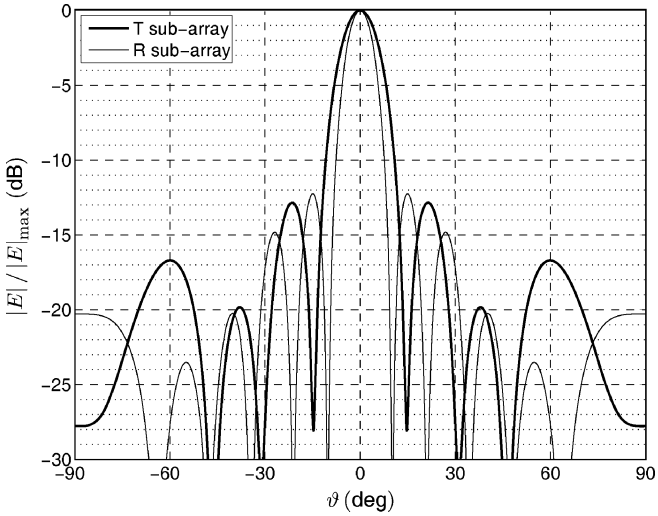

Fig. 7. The normalized sub-array patterns in the E-plane.

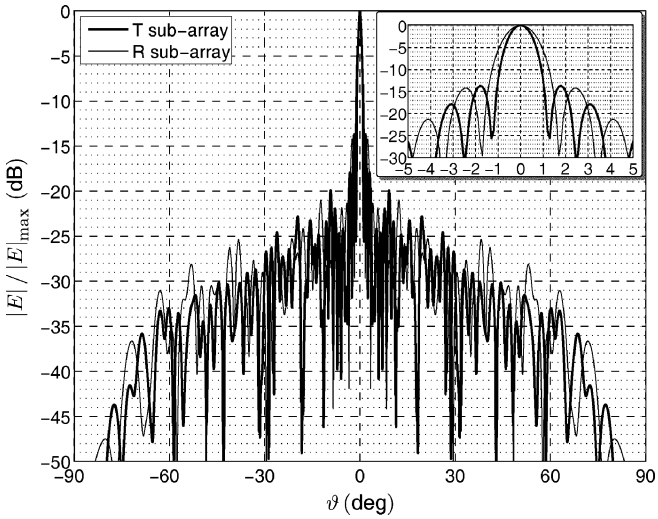

Fig. 8. The normalized sub-array patterns in the H-plane. The inset depicts a zoom-in on the main beam.

turns out to be approximately constant in the E-plane and to have a very limited variation in the H-plane, with values ranging between -32.89 dB and -32.66 dB. Summarizing, the already demonstrated adequate radiation properties of the trimmed arrays are also stable over a wide bandwidth, largely exceeding that required by the targeted application.

V. Conclusion

An effective strategy for the design of interleaved transmit and receive antennas for FMCW radar systems was presented. It involves a

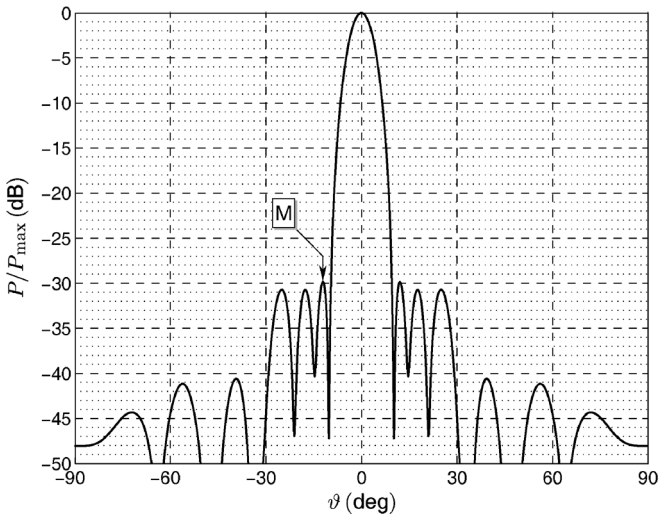

Fig. 9. The normalized, two-way pattern in the E-plane.

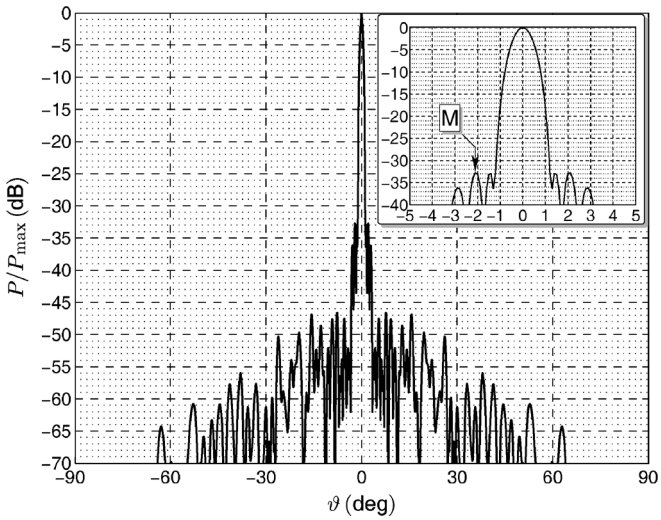

Fig. 10. The normalized, two-way pattern in the H-plane. The inset depicts a zoom-in on the main beam.

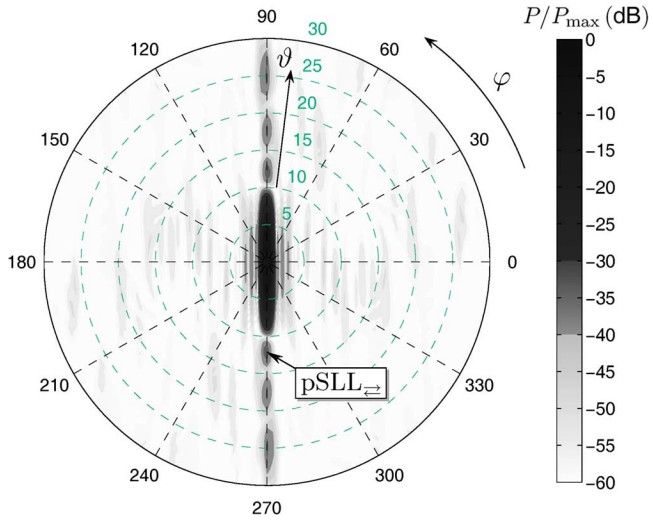

Fig. 11. The normalized, two-way pattern for $\vartheta \in [0°, 30°]$ and $\varphi \in [0°, 360°)$ at the center frequency $f_c = 9.4$ GHz.

preliminary complementary division of an initial fully populated, uniform antenna array by means of a CDS based, deterministic placement method. In a second stage, reduced numbers of columns and rows are removed from the obtained sub-arrays. The shifting of the side-lobes yielded by the elimination of columns and rows results in a drastic reduction of the peak two-way SLL. The beneficial performance of the aggregate transmit and receive front-ends is stable over a wide bandwidth, recommending the relevant shared aperture antenna for high-resolution FMCW radar applications.

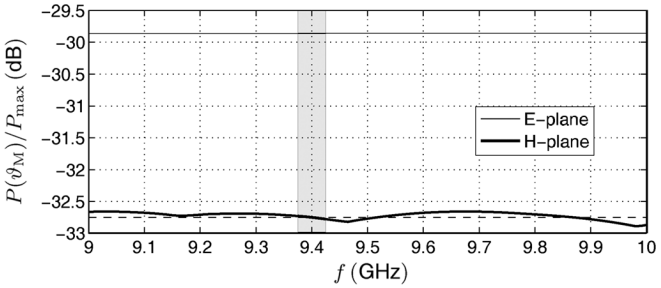

Fig. 12. The frequency variation of the normalized $\mathrm{pSLL}_{\rightleftarrows}$ in the E- and H-planes. The shaded area corresponds to the envisaged full chirp of the FMCW radar system. The dashed line represents the normalized $\mathrm{pSLL}_{\rightleftarrows}$ at the center frequency $f_c = 9.4$ GHz and in the H-plane.

ACKNOWLEDGMENT

The authors express their gratitude to Dr. A. G. Roederer of the European Space Agency—European Space Research and Technology Centre, Noordwijk, The Netherlands for his valuable suggestion concerning the reduction of the peak SLL. The authors would also like to express their thanks to the reviewers for their careful reading of the manuscript and their constructive suggestions for the improvement of this work.

REFERENCES

[1] R. L. Haupt, "Interleaved thinned linear arrays," *IEEE Trans. Antennas Propag.*, vol. 53, pp. 2858–2864, Sep. 2005.
[2] C. I. Coman, I. E. Lager, and L. P. Ligthart, "The design of shared aperture antennas consisting of differently sized elements," *IEEE Trans. Antennas Propag.*, vol. 54, pp. 376–383, Feb. 2006.
[3] C. I. Coman, I. E. Lager, and L. P. Ligthart, "Multifunction antennas—The interleaved sparse sub-arrays approach," in *Proc. 36th Eur. Microw. Conf.—EuMC*, Manchester, UK, Sep. 2006., pp. 1794–1797.
[4] A. G. Stove, "Linear FMCW radar techniques," *Proc. Inst. Elect. Eng. F*, vol. 139, pp. 343–350, Oct. 1992.
[5] M. I. Skolnik, *Radar Handbook*, 2nd ed. New York: McGraw-Hill, 1990.
[6] D. G. Leeper, "Isophoric arrays—Massively thinned phased arrays with well-controlled sidelobes," *IEEE Trans. Antennas Propag.*, vol. 47, pp. 1825–1835, Dec. 1999.
[7] S. W. Golomb and G. Gong, *Signal Design for Good Correlation: For Wireless Communication, Cryptography, and Radar*, Cambridge ed. U.K.: Cambridge Univ. Press, 2005.
[8] C. A. Balanis, *Antenna Theory: Analysis and Design*, 2nd ed. New York: Wiley, 1997, pp. 258–271.
[9] P. Gaal and S. W. Golomb, "Exhaustive determination of (1023, 511, 255)-cyclic difference sets," *Math. Comput.*, vol. 70, pp. 357–366, Mar. 2000.
[10] D. Gordon, La Jolla cyclic difference set repository [Online]. Available: www.ccrwest.org/diffsets.html